Derivative Kernels: Numerics and Applications

Mahdi S. Hosseini, *Member, IEEE*, and Konstantinos N. Plataniotis, *Fellow, IEEE*

Abstract—A generalized framework for numerical differentiation (ND) is proposed for constructing a finite impulse response (FIR) filter in closed form. The framework regulates the frequency response of ND filters for arbitrary derivative-order and cutoff frequency selected parameters relying on interpolating power polynomials and maximally flat design techniques. Compared with the state-of-the-art solutions, such as Gaussian kernels, the proposed ND filter is sharply localized in the Fourier domain with ripple-free artifacts. Here, we construct 2D MaxFlat kernels for image directional differentiation to calculate image differentials for arbitrary derivative order, cutoff level and steering angle. The resulted kernel library renders a new solution capable of delivering discrete approximation of gradients, Hessian, and higher-order tensors in numerous applications. We tested the utility of this library on three different imaging applications with main focus on the unsharp masking. The reported results highlight the high efficiency of the 2D MaxFlat kernel and its versatility with respect to robustness and parameter control accuracy.

Index Terms—MaxFlat design, low pass/full band FIR filter, high order derivatives, directional differentiation, image interpolation, Canny edge detection, image sharpening.

I. Introduction

D ERIVATIVE approximation is the hardcore problem of variety of image processing tasks. It has been utilized by various orders applied in the context of many problems including but not limited to enhancement/sharpening [1]–[3], edge detection [4], [5], curvature estimation [6], [7], local descriptors [8]–[11], and many more. The Gaussian kernels are used in a great extent for numerical implementation of such applications due to (a) simple analytical formulation of the finite impulse response (FIR) filter, (b) adaptation in different scale-space operation, and (c) similarities to the human visual system [8]. Despite its popularity, the Gaussian is mainly suitable to encode smooth-textures, but not but fine-texture images. Regardless of different scales, it is mostly accurate on low-frequency transforms and attenuates the majority of frequency spectrum that are not necessarily the representatives of noise/aliasing artifact. In fact, when it comes to the task of numerical differentiation, we face the dilemma of eliminating such contaminant artifacts or increasing the numerical accuracy of high frequency information. This dilemma fits in the context of "lowpass differentiation" to balance out these two alternatives.

In this paper, we study the problem of designing lowpass FIR differentiation that is of broad interest in signal and image processing. The key concept behind designing such a framework is to regulate derivative response (in the Fourier domain) to balance out three main principles: (a) set a custom range of solutions for wide cutoff frequencies $0 \leq \omega_c \leq \pi$, (b) maintain sharp roll-off factor by minimizing the transition band, and (c) observe free-residual artifact on the stop-band. The union of these three in one framework is pretty unique that makes the design very attractive by increasing the approximation accuracy on the pass-band, and at the same time, minimizing the impact of noise and perturbing artifacts on the stop-band. This is critical for accurate estimation of features in visual contents that are comprised of fine-textures and hence a careful treatment is required. In addition, we study the problem of designing two–dimensional (2D) kernels for directional image differentiation. Particular cases of such analysis emerge in directional-gradient (first order) or tensor-based approaches (including second order) to analyze directional structures in images. Recent advances reveal the direct applications in edge/feature detection [12], [13], pattern analysis [14], [15], and image enhancement [16].

A. Previous Works

The early work on lowpass differentiation goes back to the least-square approach by Lanczos [17], [18] which truncates high frequency harmonies in the Fourier domain while minimizing the energy of Gibbs oscillations. The method has been generalized later in [19]–[22]. Savitzky-Golay [23]–[26] are the successors of such design that have been applied in many engineering problems. The design is based on the power polynomials that fits the solution of FIR filter coefficients in a Vandermonde system of equations. The design is highly flexible in terms of varying derivative orders and cutoff frequency parametrization. However, the design contains side-lobe artifacts on the stop-band and cause hallucinated lines on the image edges that is closely tied with human visual perception error. A better noise treatment has been made by Kaiser [27], [28] using sinc interpolation or by Jacobi polynomials in [29]. Both methods, however, are limited by cutoff range designs and derivative orders. High derivative orders are also studied by Simoncelli et al [30]–[32] using sinc interpolations, or by cubic interpolating polynomials in [33]–[35]. Gaussian based kernels are also comprehensively

studied in many scale-space operations in [8], [9], [36]–[41]. A common disadvantage to all of them is they provide limited cutoff range solutions manifested by slow-decay response, causing perturbing artifacts on the stop-band.

Perhaps, a more sophisticated approach of lowpass differentiation can be addressed by Seselsnick et al [42]–[45] designed by MaxFlat technique which provides wide cutoff range with free-residual artifacts on the stop-band. The solution method, however, is limited to only zero (interpolating filter) and first order differentiation. The core idea was first introduced by Herrmann in his 1970 paper [46] to design a linear-phase lowpass FIR filter (type-I) according to the maximally flat sense such that (a) the filter traces the ideal trajectory up to a certain cutoff level, and (b) stop-band is suppressed by flattening the response tangent to zero to yield lowpass filter with ripple-free residuals. The closed form solution is accommodated by Hermite interpolating polynomials [46] and generalized in the following work by Daubechies [47], Seselsnick [42]–[44], Cooklev [48], [49], Samadi [50], and Pei [51]. The capability of vanishing *"undesired"* frequencies in a flexible cutoff range with sharp localized responses is indeed a viable asset for image analysis. Contourlet transforms are of such examples that utilize MaxFlats for multi-scale analysis [52].

B. Shortcomings and Contributions

Despite vigorous research efforts, it comes as a surprise to note that the construction of lowpass FIR derivative filters within the MaxFlat framework is limited only up to first order differentiation [45]. To the best of our knowledge, there is no formulation of second and higher orders in the literature that can, similar to first order in [45], set a custom range of cutoff frequency with sharp decay and ripple-free residuals. This is mainly because the derivation of closed form solutions for higher order is not a feasible task by means of the methods such as power series expansions in [45]. The difficulty lies in solving a non-homogeneous high order nonlinear differential equations which is almost impractical.

In this paper we take a different approach to complement this design by incorporating the method of undetermined coefficients as a stencil model into the MaxFlat framework. Accommodated by the Fourier transform and Taylor series expansion, we transform the associated variables and we establish a direct link between the interpolating polynomials and filter response to propose a generalized framework. The contributions of this work are in three folds:

- We find a comprehensive list of solutions in a matrix-vector linear system of equation for arbitrary derivative orders with customized lowpass/fullband filter design. We offer the exact solution by using symbolic calculations in MATLAB for computer programming.
- We employed the proposed MaxFlat filters in two dimensional (2D) directional differentiation kernel designs that can be tuned for arbitrary derivative orders, cutoff frequencies, and rotating (steering) direction. These 2D MaxFlat kernels offer superior performance compared to that of steerable gradient design using Gaussian filters [12], [37] applied to image feature extraction.
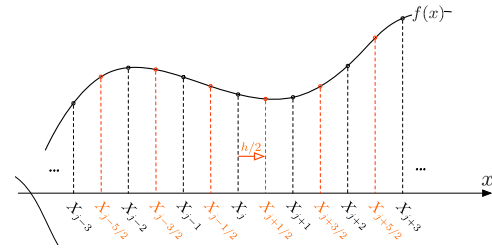

Fig. 1. Equidistant mesh grids and staggered nodes by a halfway sample shift ($h/2$).

- We studied the utility of the 2D MaxFlat kernels in three different applications of image interpolation, Canny edge detection and unsharp masking as variants of different derivative orders. The numerical evaluations of the proposed solutions outperform the state-of-the-art results.

The remainder of this paper is structured as follows. We formulate the problem of lowpass FIR differentiation in a generalized framework in Section II. The utility of the proposed framework is studied in Section III. The calculated filters are employed in directional differentiation in Section IV, whereas the applications are reported in Section V. Concluding remarks are discussed in Section VI.

II. PROPOSED NUMERICAL FRAMEWORK

The numerical difference models constraint by undetermined coefficients has been studied abundantly to derive set of solutions to fullband FIR differentiation by means of Taylor or Lagrangian expanding series [53]–[61]. In this section, we incorporate this model to transfer the variables into Fourier domain and regulate the filter response by means of maximally-flat criterion. The proposed approach not only benefits from including arbitrary differential orders, but also integrates a parameter control to manipulate various cutoff levels.

A. Undetermined Coefficients

Let $\Omega = [a, b]$ and f be a function $f(x) : \Omega \mapsto \mathbb{R}$, and assume that f is continuous from first to nth derivatives i.e. $f(x) \in C^n$, with n being as large as necessary. The function values, which are also known as *nodal values*, are prescribed around a node X_j with equidistant grids (uniform sampling) i.e. $X_{j\pm k} = X_j \pm \ell_k h$, where $k \in \{1, \ldots, L\}$ and ℓ_k is defined either at exact nodes $\ell_k = k$ or staggered position $\ell_k = k - \frac{1}{2}$ known as half-sample delay [62]. Figure 1 demonstrates the lattice nodes with h being the sampling interval for discretization known as the *sampling rate*.

The odd and even interpolants are defined by

$$p_o^{j,k} \triangleq \frac{f_{j+\ell_k} - f_{j-\ell_k}}{2} = \sum_{n=0}^{\infty} \frac{(\ell_k h)^{2n+1}}{(2n+1)!} f_j^{(2n+1)}, \quad \text{(1a)}$$

$$p_e^{j,k} \triangleq \frac{f_{j+\ell_k} + f_{j-\ell_k}}{2} - 1 = \sum_{n=1}^{\infty} \frac{(\ell_k h)^{2n}}{(2n)!} f_j^{(2n)}. \quad \text{(1b)}$$

where $f_j = f(x)\big|_{x=X_j}$. Furthermore, the right hand sides of equations (1a)-(1b) are obtained by Taylor series expansion.

Accordingly, the odd and even derivatives are synthesized by means of linear interpolation

$$f_j^{(2m+1)} = \sum_{k=1}^{L} c_k p_o^{j,k}, \quad m \in \{0, 1, \ldots\} \tag{2a}$$

$$f_j^{(2m)} = \sum_{k=1}^{L} c_k p_e^{j,k}, \quad m \in \{1, \ldots\}. \tag{2b}$$

where c_k is the coefficient to be determined.

B. Frequency Regulation: Rise of Maximally-Flat Sense

We can obtain corresponding transfer functions (filter response) of (2a)-(2b) by discrete Fourier transform (DFT)

$$H^{2m+1}(\omega) \triangleq \frac{\mathcal{F}\{f^{(2m+1)}\}}{\mathcal{F}\{f_j\}} = i \sum_{k=1}^{L} c_k \sin \ell_k h\omega \tag{3a}$$

$$H^{2m}(\omega) \triangleq \frac{\mathcal{F}\{f^{(2m)}\}}{\mathcal{F}\{f_j\}} = \sum_{k=1}^{L} c_k (\cos \ell_k h\omega - 1). \tag{3b}$$

With two possibilities of centralized/staggered nodes for ℓ_k, we can construct four different cases similar to the generalized cases in [48]. In particular, we are only interested in (a) $\ell_k = k - 1/2$ for odd (anti-symmetric), and (b) $\ell_k = k$ for even (symmetric) order of differentiations. This is to avoid deviation of high-frequencies when high cutoff is needed.

Associated with the transfer functions in (3a)-(3b), we impose the following constraints to approximate the ideal-lowpass FIR differentiators in the maximally-flat sense

$$\frac{d^p H^n(\omega)}{d\omega^p}\bigg|_{\omega=0} = \frac{d^p H_c^n(\omega)}{d\omega^p}\bigg|_{\omega=0}, \quad p \in \{0, \ldots, P\} \tag{4a}$$

$$\frac{d^q H^n(\omega)}{d\omega^q}\bigg|_{\omega=\pi} = 0, \quad q \in \{0, \ldots, Q\}. \tag{4b}$$

where P and Q are the free parameters controlling the tangent power at low and high frequencies, respectively. $H_c^n(\omega)$ in (4a) refers to the continuous Fourier transform of the ideal nth order derivative function defined by $H_c^n(\omega) = \hat{f}^{(n)}(\omega)/f(\omega) = (i\omega)^n$. Substituting the odd form of this transfer function yields $H_c^{2m+1}(\omega) = i(-1)^m \omega^{2m+1}$ which is purely imaginary. Similarly, the substitution for even form yields $H_c^{2m}(\omega) = (-1)^m \omega^{2m}$ which is purely real.

Before applying the MaxFlat constraints in (4a)-(4b) on the transfer functions (3a)-(3b), we decompose the sinusoid terms by means of Taylor-Maclaurin series expansion at particular frequency point ω_0 by

$$\sin (\ell_k(\omega - \omega_0)) = \sum_{n=0}^{\infty} \frac{(-1)^n}{(2n+1)!} (\ell_k(\omega - \omega_0))^{2n+1}$$

$$\cos (\ell_k(\omega - \omega_0)) = \sum_{n=0}^{\infty} \frac{(-1)^n}{(2n)!} (\ell_k(\omega - \omega_0))^{2n}.$$

Calculating the pth derivative of the above expansions results in

$$\frac{d^p}{d\omega^p}\{\sin (\ell_k(\omega - \omega_0))\} = \sum_{n=0}^{\infty} \frac{(-1)^n \ell_k^{2n+1}}{(2n+1-p)!} (\omega - \omega_0)^{2n+1-p}$$

$$= \begin{cases} (-1)^n \ell_k^{2n+1}, & p = 2n+1 \\ 0, & \text{else} \end{cases} \tag{6}$$

and

$$\frac{d^p}{d\omega^p}\{\cos (\ell_k(\omega - \omega_0))\} = \sum_{n=0}^{\infty} \frac{(-1)^n \ell_k^{2n}}{(2n-p)!} (\omega - \omega_0)^{2n-p}$$

$$= \begin{cases} (-1)^n \ell_k^{2n}, & p = 2n \\ 0, & \text{else.} \end{cases} \tag{7}$$

Now by substituting (3a) in MaxFlat constraints (4a)-(4b) and accommodating the sinusoid terms using the trigonometric expansion in (6), we derive the following system of linear equations for odd numerical differentiation

$$\sum_{k=1}^{L} \ell_k^{2p+1} c_k = \begin{cases} 0, & p \in \{0, 1, \ldots, \lfloor \frac{P-1}{2} \rfloor\} \setminus \{m\} \\ (2m+1)!, & p = m \end{cases} \tag{8a}$$

$$\sum_{k=1}^{L} (-1)^k \ell_k^{2q} c_k = 0, \quad q \in \{0, 1, \ldots, \lfloor \frac{Q}{2} \rfloor\} \tag{8b}$$

The linear sets of equations (8a)-(8b) are the translation of MaxFlat criterion to hold the tangency of low and high frequency responses at $\omega = \{0, \pi\}$. The uniqueness of the solution in (8a)-(8b) is satisfied if $\lfloor \frac{P-1}{2} \rfloor + \lfloor \frac{Q}{2} \rfloor + 2 = L$.

Finally, associated by the trigonometric expansion in (7), the corresponding system of linear equations for even numerical differentiation are obtained by substituting (3b) in (4a)-(4b) and yield

$$\sum_{k=1}^{L} \ell_k^{2p} c_k = \begin{cases} 0, & p \in \{1, \ldots, \lfloor \frac{P}{2} \rfloor\} \setminus \{m\} \\ (2m)!, & p = m \end{cases} \tag{9a}$$

$$\sum_{k=1}^{L} \left((-1)^k - 1\right) c_k = 0, \tag{9b}$$

$$\sum_{k=1}^{L} (-1)^k \ell_k^{2q} c_k = 0, \quad q \in \{1, \ldots, \lfloor \frac{Q}{2} \rfloor\}. \tag{9c}$$

where, the uniqueness of the solution in (9b)-(9c) is satisfied if $\lfloor \frac{P}{2} \rfloor + \lfloor \frac{Q}{2} \rfloor + 1 = L$. In both odd and even design cases, different combination of P and Q controls the cutoff range of the lowpass FIR filter.

C. Matrix-Vector Formulation

We can construct the matrix-vector formulation analogues to the system of linear equations in (8a)-(8b) and (9a-9c) by

$$\begin{bmatrix} \mathbf{M}_{\lfloor \frac{P-1}{2} \rfloor} \cdot \mathbf{L} \\ \mathbf{M}_{\lfloor \frac{Q}{2} \rfloor} \cdot \mathbf{S} \end{bmatrix} \mathbf{c}_{o,m} = \mathbf{b}_o^m \tag{10a}$$
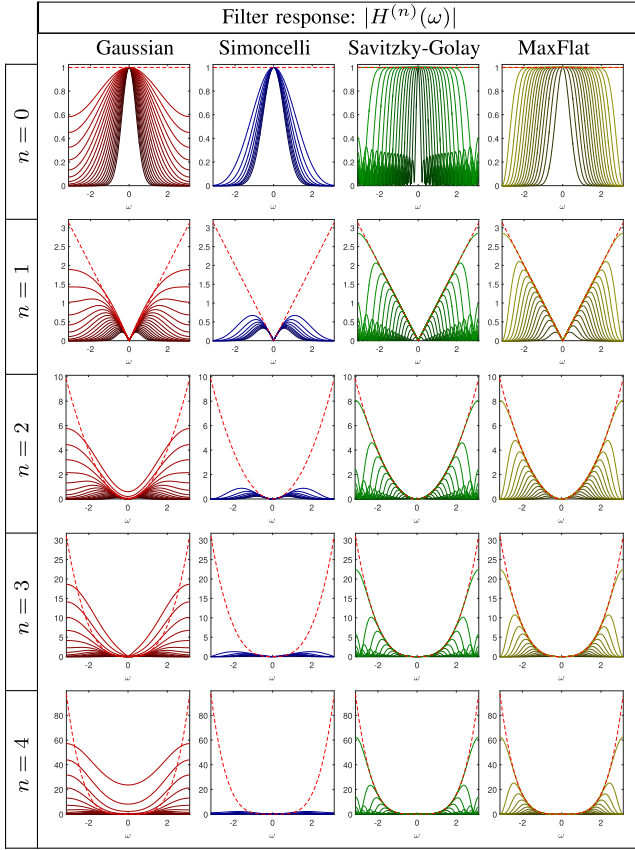
$$\begin{bmatrix} \mathbf{M}_{\lfloor \frac{P}{2} \rfloor - 1} \cdot \mathbf{L}^2 \\ \hline \text{diag } \mathbf{S} - \mathbf{1} \\ \hline \mathbf{M}_{\lfloor \frac{Q}{2} \rfloor - 1} \cdot \mathbf{L}^2 \cdot \mathbf{S} \end{bmatrix} \mathbf{c}_{e,m} = \mathbf{b}_e^m, \tag{10b}$$

where,

$$\mathbf{M}_n = \begin{bmatrix} 1 & 1 & \ldots & 1 \\ \ell_1^2 & \ell_2^2 & \ldots & \ell_L^2 \\ \vdots & \vdots & \ddots & \vdots \\ \ell_1^{2n} & \ell_2^{2n} & \ldots & \ell_L^{2n} \end{bmatrix},$$

TABLE I

LOWPASS FIR DERIVATIVE RESPONSES OF ZERO, FIRST, SECOND, THIRD, AND FOURTH ORDERS BY MEANS OF FOUR DIFFERENT METHOD DESIGNS OF GAUSSIAN, SIMONCELLI [30]–[32], SAVITZKY-GOLAY [23]–[26], AND PROPOSED MAXFLAT FILTERS. TRANSITION OF COLOR SHADES FROM DARK TO BRIGHT ARE ACHIEVED BY TWEAKING THEIR CORRESPONDING TUNING PARAMETERS TO MANIPULATE DIFFERENT RANGE OF CUTOFF FREQUENCIES. THE BALANCED CUTOFF RANGE SOLUTIONS, SHARP ROLL-OFF FACTOR, AND FREE-RESIDUAL ARTIFACTS ON THE STOP-BAND IN MAXFLAT ARE HIGHLY EVIDENT COMPARED TO OTHER METHODS
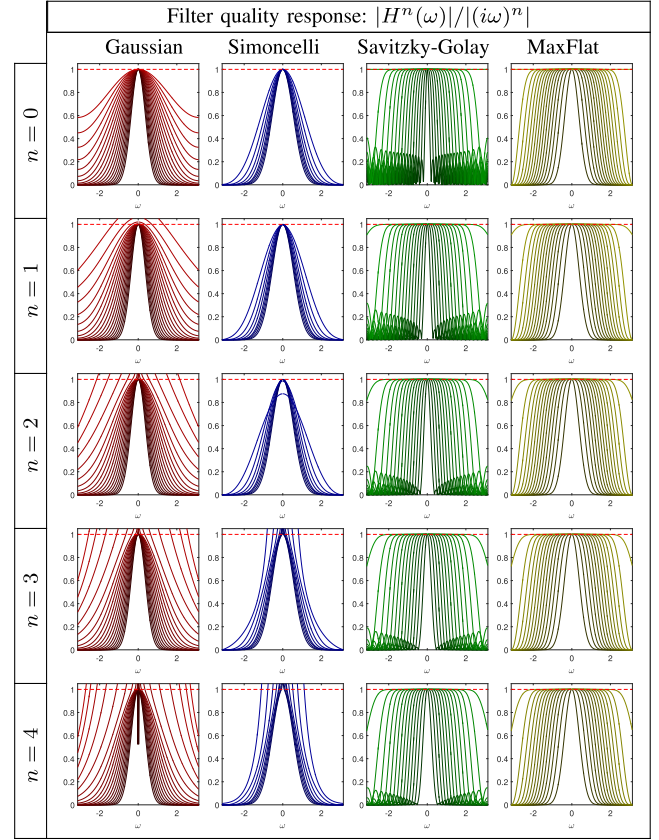

TABLE II

FILTER QUALITY RESPONSES OF ZERO, FIRST, SECOND, THIRD, AND FOURTH ORDER LOWPASS FIR DERIVATIVES INTRODUCED IN TABLE I

are constructed by odd length ($N = 2L + 1$)/symmetric form (case-I)

$$\mathbf{d}_{2m} = \left[\mathbf{c}_{e,m}, -2 \sum_{k=1}^{L} \mathbf{c}_{e,m}(k), \mathbf{c}_{o,m} \right]^T, \qquad (12)$$

where the vector coefficient $\mathbf{c}_{e,m}$ is defined by (10b).

D. Exact Solution by Symbolic Calculation

The structure of matrices in (10a)-(10b) is a partitioned block Vandermonde matrix that are highly ill-conditioned (numerically unstable). Nevertheless, Vandermonde matrices in general are non singular and a closed form solution exists [63]. We solve this partitioned systems using MATLAB' symbolic toolbox with reasonable tap-length size $L \leq 50$ in ordinary desktop machines, which is practically feasible to provide reasonable cutoff resolutions. Table I demonstrates variants of lowpass FIR derivative filters using our proposed MaxFlat filters. Furthermore, we select three other filters from the literature, namely Gaussian, Simoncelli [30]–[32], and Savtizky-Golay filters [23]–[26] to compare their performances. The cutoff level for the Gaussian kernels is tuned by the variance parameter (σ). Simoncelli's filters do not contain any tuning parameter but its corresponding cutoff can be manipulated by the filter tap-length. The Savitzky-Golay on the other hand, directly controls the cutoff

$\mathbf{S} = \mathrm{diag}\left((-1)^i\right)$ and $\mathbf{L} = \mathrm{diag}(\ell_i)$ are squared diagonal matrices of size L. Both $\mathbf{b}_o^m = [0, \dots, (2m + 1)!, \dots, 0]^T$ and $\mathbf{b}_e^m = [0, \dots, (2m)!, \dots, 0]^T$ contains one non-zero entry at $(m + 1)$th row. The systems of equations in (10a)-(10b) include FIR coefficient design for different (a) order of differentiation defined by m, (b) filter tap-length defined by L, and (c) cutoff frequency controlled by combinations of P and Q. Accordingly, the odd order of differentiation is constructed by even length ($N = 2L$)/anti-symmetric structure (case-IV)

$$\mathbf{d}_{2m+1} = \left[\mathbf{c}_{o,m}, -\mathbf{c}_{o,m} \right]^T, \qquad (11)$$

where, the vector coefficient $\mathbf{c}_{o,m}$ is determined by (10a). Note that $\mathbf{d}_o^m$ estimates the derivatives at staggered nodes, and, therefore, it can be implemented either in backward $[\mathbf{d}_o^m, 0]$ or forward $[0, \mathbf{d}_o^m]$ schemes, causing $h/2$-shift back or ahead, respectively. Similarly, the FIR coefficients of even derivatives

TABLE III

PERFORMANCE ANALYSIS OF LOWPASS DERIVATIVE FIR FILTERS BY MEANS OF FOUR DIFFERENT METHODS OF GAUSSIAN, SIMONCELLI, SAVTIZKY-GOLAY, AND MAXFLAT (PROPOSED). FIRST TO THIRD COLUMNS OF THIS TABLE SHOW THE CUTOFF RANGE SOLUTION INCLUDING THE TRANSITION BAND AS PER FUNCTIONS OF TUNING PARAMETERS FOR ZERO, FIRST, AND SECOND ORDER DIFFERENTIATION. THE FOURTH TO SIXTH COLUMNS DEMONSTRATE THE SPECTRAL POWER DENSITY CONSUMPTION OF PASS-BAND COMPARED TO THEIR STOP-BAND ON THE SAME DERIVATIVE ORDERS. MAXFLAT FILTERS PROVIDE A BALANCED DESIGN OF WIDE CUTOFF FREQUENCY, MINIMAL TRANSITION BAND, AND MINIMAL ENERGY CONSUMPTION ON THE STOP-BAND COMPARED TO ALL THREE COUNTERPART SOLUTIONS
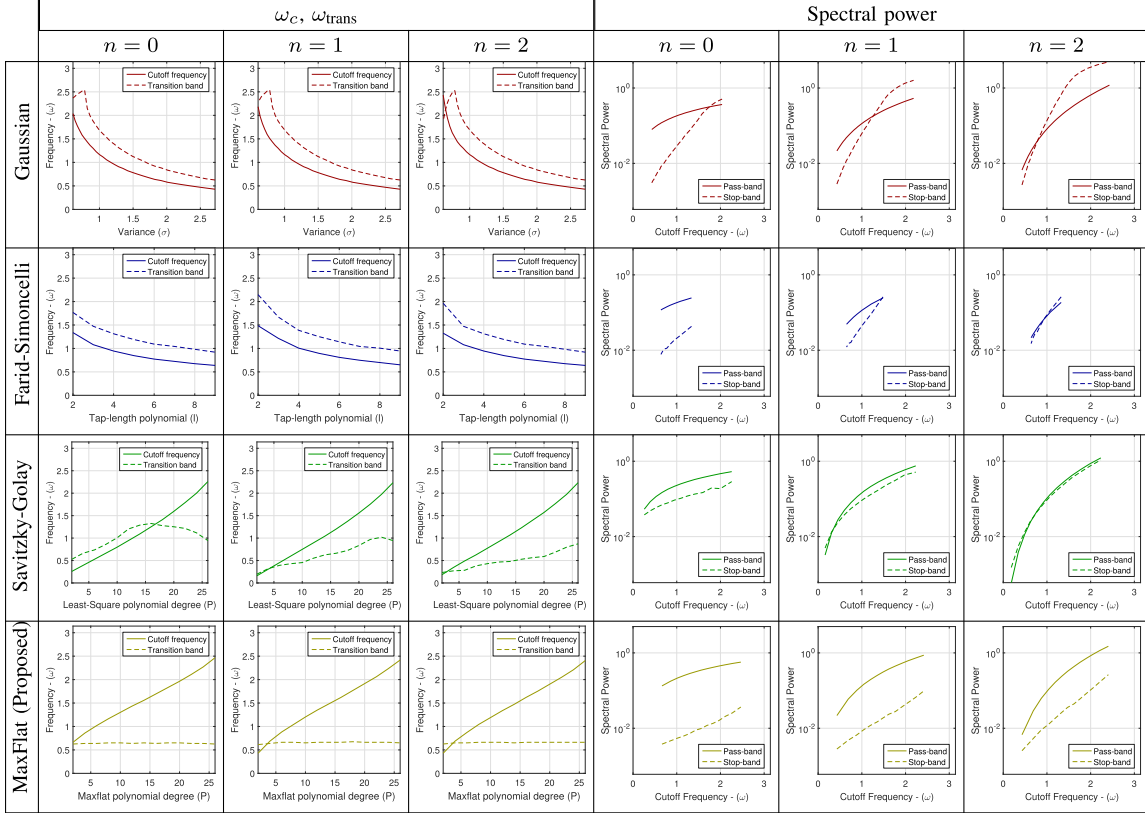
level by the polynomial degree, similar to the tuning parameter P used in MaxFlat design. The Gaussian mainly suffers from wide transition band on the high cutoff frequencies. Simoncelli provides limited cutoff range and Savitzky-Golay contains side-lobe artifacts on the stop-band. In contrast to all three, the MaxFlat filters solve these issues in a more balanced way.

To better realize this improvement, the filter qualities are also demonstrated in Table II that are obtained by the relative ratio of the discrete response to the continuous case $\frac{|H^n(\omega)|}{|(i\omega)^n|}$. Here, an appropriate lowpass filter is referred to the one that either preserves a designated frequency (quality equals to one) or eliminates it (quality equals to zero) with sharp roll-off factor. The relative comparison among all filters implies that the proposed MaxFlat framework is a suitable candidate for accurate tuning of wider range of cutoff frequencies.

III. ON THE UTILITY OF MAXFLAT FILTERS

To evaluate the theoretical performance of the proposed MaxFlat filters compared to three aforementioned filters, we conduct a numerical evaluation by quantifying the principles (a)-(c) defined in the introduction. The *pass-band* of an FIR filter here is referred to the frequency range bounded

by the cutoff level $0 \leq \omega_{\text{pass}} \leq \omega_c$ which is found by the halfway (3dB) attenuation of the filter quality response i.e. $|H^n(\omega)|/|j\omega|^n$ similar to the definition used in [42]–[45]. Furthermore, the *transition* band is determined between the 10% and 90% falling amplitude frequencies $\omega_a \leq \omega_{\text{trans}} \leq \omega_b$. The *stop-band* frequency is also defined beyond the 90% falling amplitude frequency $\omega_b \leq \omega_{\text{stop}} \leq \pi$.

First we validate the maximum cutoff range achieved from every individual method by varying their parameters i.e. σ for Gaussian, l for Simoncelli, and P for both Savtizky-Golay and proposed MaxFlat. The tap-length here is $L = 15$. Table III, (first to third columns) demonstrate the cutoff frequency and transition band (overlaid on top of each other) achieved as functions of tuning parameters for zero, first and second order differentiations. While both Savtizky-Golay and MaxFlat filters provide wide cutoff ranges compared to Gaussian and Simoncelli, the transition band obtained by MaxFlat remains minimal compared to all three. Though Savitzky-Golay provide sharper roll-off on transition band compared to MaxFlat, the existing side-lob artifacts contribute to longer transition period and hence falls behind the MaxFlat. Examples of the filter responses of all four methods are also shown in Table IV for two different cutoff frequencies. The artifacts on both transition-band and stop-band observed for

TABLE IV

DESIGN OF ZERO, FIRST, AND SECOND ORDER DERIVATIVE LOWPASS FIR FILTERS BY MEANS OF FOUR DIFFERENT METHODS OF GAUSSIAN, SIMONCELLI, SAVTIZKY-GOLAY, AND MAXFLAT (PROPOSED). TWO CUTOFF FREQUENCIES $\omega_c = \{0.28\pi, 0.43\pi\}$ (RAD) ARE SET TO DEMONSTRATE THE FILTERS VARIABILITY WITH RESPECT TO DIFFERENT CUTOFFS, ROLL-OFF BEHAVIOR, AND STOP-BAND ARTIFACTS. THE SHARP ROLL-OFF AND FREE RESIDUAL ARTIFACTS OF MAXFLAT APPROACH IS HIGHLY EVIDENT COMPARED TO THREE COUNTERPART SOLUTIONS
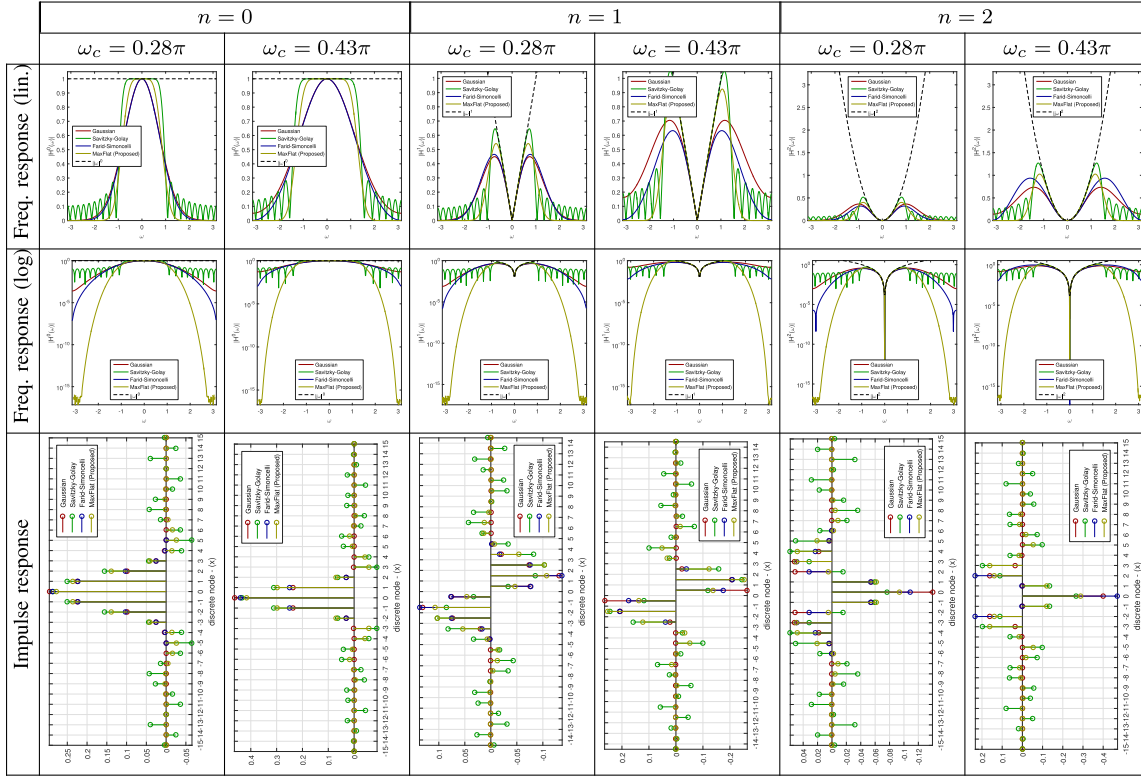
MaxFlat are very minimal compared to other three methods. This is shown by logarithmic-scale of the filter responses in the same table.

The key-roll of deploying a suitable lowpass derivative filter in practice is to make sure the perturbed artifacts introduced in stop-band has minimal effect on approximating the underlying signal/image features. To investigate this, the power spectral densities on both pass-band and stop-band of all filters are calculated. The relative comparison between these two energies provides a meaningful insight on the deviation of filter response with respect to its perturbed artifacts. In other words, calculating the leftover energy on the stop-band is a way to measure how bad the filter transformation impacts the approximation accuracy. The corresponding spectral powers are shown in Table III (fourth to sixth columns) for all four different methods. By increasing the differentiation order, the gap between pass-band and stop-band energies decreases and they become closer. This is expected since high order differentiations are more sensitive to higher frequencies as a magnitude of ω^n than lower frequencies. The relative comparison between four methods shows that the MaxFlat filters provide more efficient truncation of the stop-band energy with respect to different cutoffs. While Gaussian filters perform better on the lower cutoffs, by increasing its cutoff frequency, the concentrated energy on the stop-band reaches beyond the pass-band and becomes useless. Simoncelli filters perform similar to

the Gaussian, but with narrower cutoff range solutions. Savitzky-Golay filters on the other hand provide more robust design with respect to cutoff parameter, where the energy on the stop-band remains lower than the pass-band. This is more evident on low order derivatives. However, the gap energies are smaller than Gaussian and Simoncelli due to perturbed side-lobes on the stop-band. As a conclusion, MaxFlat filters provide more efficient designs where the rank observation of the pass-band energy is very consistent with respect to different cutoff parameters and derivative orders.
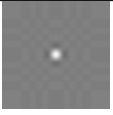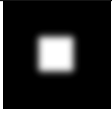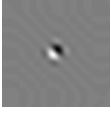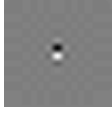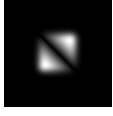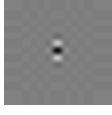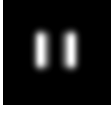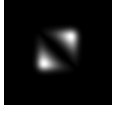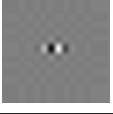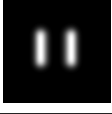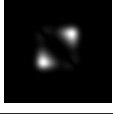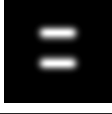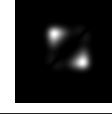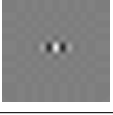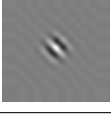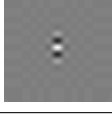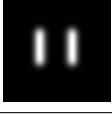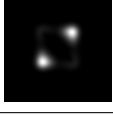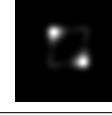
IV. IMAGE DIRECTIONAL DIFFERENTIATION

In this section we design 2D kernels to calculate high-order directional derivatives on the images. The technique of directional differentiation has been pioneered by Freeman–Adelson [37] to design steerable filters enclosed with Gaussian kernels. Examples of such kernels are provided in the supplementary materials. Our focus here is to generalize the 2D–directional differentiators by means of MaxFlat kernels proposed in previous section to obtain 2D convolution kernels that contain flexible cutoff range and sharp frequency localized responses for image analysis.

A. High-Order Directional Differentiation

Given a surface image $f(x, y) \in \mathbb{R}^{m \times n}$, the goal is to approximate the nth–order directional derivative of the surface

TABLE V

2D MAXFLAT CONVOLUTION KERNELS $K_{2D}(n, \theta, P_x, P_y)$ FOR ARBITRARY ORDER OF DIFFERENTIATION n, STEERING DIRECTION θ, AND CUTOFF FREQUENCY CONTROLLED BY FLATNESS DEGREE P. SELECTED PARAMETERS HERE ARE $L = 25$ AND $P_x = P_y = 12$ ($\frac{\omega_c}{\pi} \approx 0.3$) FOR ALL FILTERS

denoted by $D_{\vec{u}}^n f(x, y)$ along a unit vector $\vec{u} = (u_x, u_y)$. The first-order directional derivative is defined by projecting the gradient vector ∇f on $\vec{u}$ i.e. $D_{\vec{u}} f = \vec{u} \cdot \nabla f$. The linear operator $D_{\vec{u}}$ can be applied once again to obtain second-order direction i.e. $D_{\vec{u}}^2 f = D_{\vec{u}}(\vec{u} \cdot \nabla f) = \vec{u} \cdot \nabla(\vec{u} \cdot \nabla f)$. Since the gradient of a constant vector is zero $\nabla \vec{u} = 0$, then $D_{\vec{u}}^2 f = \vec{u} \cdot (\vec{u} \cdot \nabla^2 f)$. Using the same recursive approach, the nth–order directional differentiation is obtained by $D_{\vec{u}}^n f = \vec{u} \cdot (\vec{u} \cdot (\cdots (\vec{u} \cdot \nabla^n f)))$. Here, the term $\nabla^n f$ consists of $(n + 1)$-order tensor and by induction of polynomial expansion it can be simplified in the form of linear combination of partial derivatives of order n

$$D_{\vec{u}}^n f = \sum_{k=0}^{n} \binom{n}{k} u_x^{n-k} u_y^k \frac{\partial^n f}{\partial x^{n-k} \partial y^k}. \tag{13}$$

The partial derivatives $\frac{\partial^n f}{\partial x^{n-k} \partial y^k}$ in (13) with impulse response $f(x, y) = \delta(x, y)$ construct 2D-basis kernels that can be separated in two axes x and y independently such $\frac{\partial^{n-k}}{\partial x^{n-k}}\left(\frac{\partial^k \delta}{\partial y^k}\right)$. One possible approach for discrete approximation of these kernels is to accommodate each partial differentiator, either in x or y, by means of the MaxFlat lowpass derivative filters proposed in previous section. Hence, the corresponding 2D–basis can be approximated by $\frac{\partial^n \delta}{\partial x^{n-k} \partial y^k} \approx \mathbf{d}_k^T \mathbf{d}_{n-k}$, where $\mathbf{d}_n$ is defined in (11) and (12) for odd and even differentiators, respectively. Note that $n = 0$ corresponds to only lowpass filter. Assuming the projection is defined on a polar direction $\vec{u} = (\cos\theta, -\sin\theta)$ with anti-clockwise rotation, the final discrete approximation of the directional differentiator $D_{\vec{u}}^n \delta$ can be represented by the
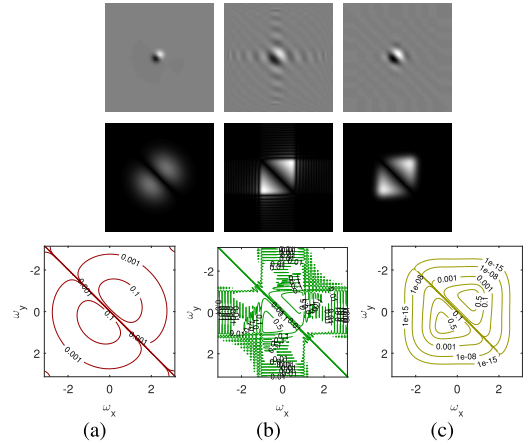
Fig. 2. First order directional derivative kernels rotated at $\theta = \pi/4$ and cutoff $\omega_c = 1$ (rad). Impulse response are shown in first row, frequency response in second row, and contour level of the frequency response in third row. (a) Gaussian. (b) Savitzky-Golay. (c) MaxFlat.

following 2D–convolution kernel

$$K_{2D}(n, \theta, P_x, P_y) = \sum_{k=0}^{n} (-1)^k \binom{n}{k} \cos^{n-k}\theta \sin^k\theta \; \mathbf{d}_k^T \mathbf{d}_{n-k}. \tag{14}$$

The above kernel design includes arbitrary order of differentiation 'n' in a predefined rotating angle 'θ' and cutoff frequency levels controlled by 'P_x' and 'P_y' that are tuned separately for both axes x and y, respectively.

Table V displays a few 2D MaxFlat kernels both in spatial and frequency domain up to fourth OD with four

(a) Original   (b) Bicubic: PSNR $= 34.55$ (c) G: PSNR $= 32.94$

(d) S: PSNR $= 32.16$ (e) SG: PSNR $= 32.42$ (f) M: PSNR $= 36.25$ (g) SRCNN: PSNR $= 37.48$

Fig. 3. Single image up-sampling from down-sampled version of Curiosity image by scale factor of two using bi-cubic [64], Gaussian (G), Simoncelli (S), Savitzky-Golay (SG), and MaxFlat (M) interpolating kernels shown in (b)-(f). Results of super-resolution problem using SRCNN [13] is also shown in (g).

different steering directions $\theta = \{0, \frac{\pi}{4}, \frac{\pi}{2}, \frac{3\pi}{4}\}$. The sharp localization in frequency domain is apparent. At the lowest derivative level $n = 0$, which is equivalent to a lowpass (interpolation) filter, the kernel is non-directional. Here the filter order is set to $L = 25$ and flatness degree to $P_x = P_y = 12$ for all cases. Accordingly, the corresponding cutoff frequency level for this flatness degree is $\omega_c = 0.3\pi$ similar to the function-profile obtained in Table III. For numerical implementation in computer programming, such as MATLAB, the directional differentiation of an image `I` can be formulated by means of two-dimensional convolution problem `imfilter(I, K_{2D}, 'boundary')` function, where `I` is the input image, K_{2D} is the 2D MaxFlat kernel, and `'boundary'` is the boundary–condition. The relative performance of the proposed MaxFlat kernel compared to the steerable Gaussian [37] and Savitzky-Golay filters are also shown in Figure 2. The kernels are the first order differentiators rotated at $\theta = \pi/4$ with cutoffs set at $\omega_c = 1$ radian. As it shown, the Gaussian provides slow decay response and Savitzky-Golay contains ripple artifacts at the stop-band. In contrast, the MaxFlat provides a balanced response with sharp decay and free artifact on the stop-band.

V. APPLICATIONS

In this section, we present the results achieved by applying the proposed 2D MaxFlat kernels in three applications i.e. image interpolation, edge detection, and unsharp masking to study the utility of zero, first, and second orders of differentiations, respectively. Throughout these applications the terms of evaluation for quality assessment of a reconstructed image are selected among three measurements: two reference-based indexes using (a) peak-signal-to-noise-ratio (PSNR) which is sensitive to statistical deviation of pixel-to-pixel match, and (b) mean structural similarity index measure (MSSIM) which is sensitive to geometrical miss-matches [65], and one

non-reference based metric using (c) sharpness index (SI) which is sensitive to image blurriness [66], [67]. For better visual judgment of the generated images the smoothing effect from the viewer software e.g. Adobe Acrobat should be turned off.

A. Image Interpolation: Variant of Zero Order Derivative

Image interpolation is a classical problem referring to recovering high-resolution image (up-sampled) image from its under-sampled version in a single-image based level [13], [64]. A test image is first down-sampled by means of a lowpass (interpolating) filter and then up-sampled back using the same filter to compare the recovery image from its original image.

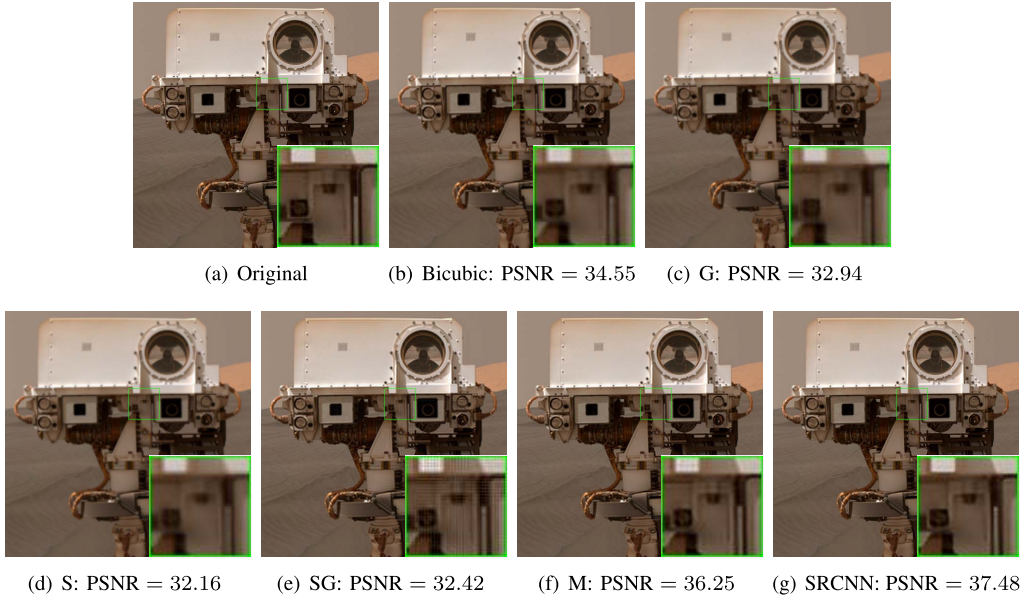Our aim in this section is to study the utility of different zero-order ($n = 0$) lowpass filters introduced in previous section. The experiments here are conducted on the Curiosity image[1] shown in Figure 3(a). The image is down-sampled by scale-factor of two and up-sampled back using different interpolation filters: (a) bi-cubic [64] (`imresize` build-in function in MATLAB), (b) zero-order lowpass derivatives of Gaussian, Simoncelli, Savitzky-Golay, and MaxFlat with cutoff frequencies set at $\omega_c = \pi/2$. To obtain relative cutoff frequency by means of different lowpass filters, refer to Section III for more detail explanation on how the pertinent parameters should be tuned to achieve certain cutoff levels. Furthermore, we adopt the sixth comparison method using multilayer decomposition approach in [13] known as the method of super resolution convolution neural network (SRCNN). This method creates a mapping between low and high-end resolution images using deep convolutional neural network (CNN). The mapping accepts the up-sampled bi-cubic interpolated image shown

[1]PIA20316: Curiosity self-portrait at Martian Sand Dune taken in Jan 19, 2016. A 512×512 tile is cropped from the original TIFF format available online at http://photojournal.jpl.nasa.gov/targetFamily/Mars.
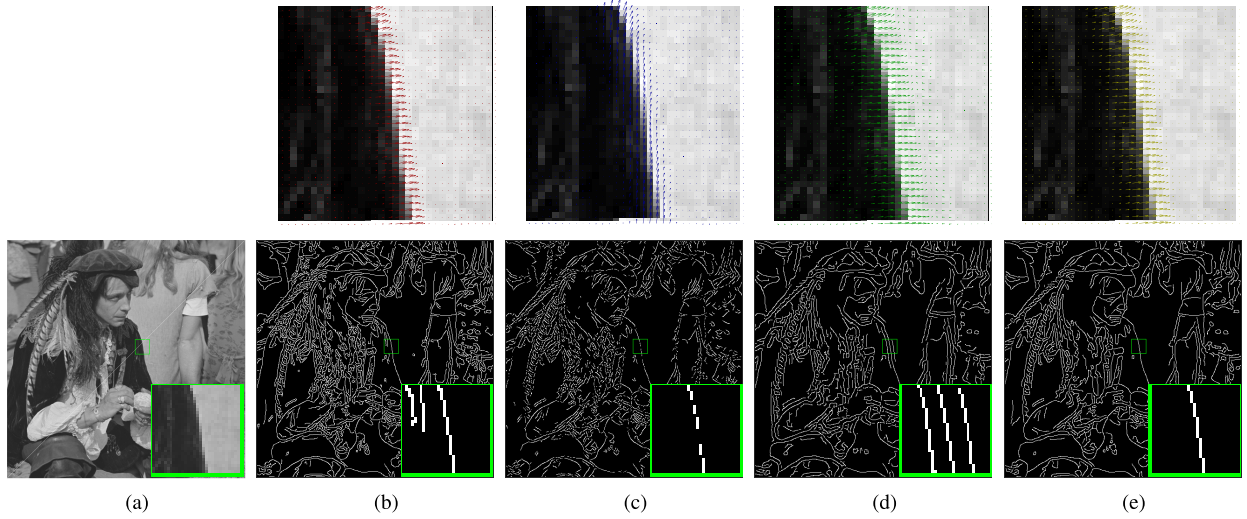
Fig. 4.   Canny edge detection performance by means of four different derivative kernels. The cutoff frequency is set to $\omega_c = 0.75$ (rad). The top images corresponds to the velocity vectors overlaid on selected image patch as arrows of gradient components $\{\partial I/\partial x, \partial I/\partial y\}$. (a) Original Image. (b) Gaussian. (c) Simoncelli. (d) Savitzky-Golay. (e) proposed MaxFlat.

in Figure IV-A as an input and breaks it down to multiple patches for sparse exploration by means of three decomposing layers. The network is trained prior in advance to optimize the decomposition filters for reconstruction. The result of reconstruction using the above methods are shown in Figure 3. The means of evaluation here is PSNR and according to the rank observation, SCRNN and MaxFlat perform better with better visual quality as opposed to the other approaches. Though SRCNN is performing better than MaxFlat, it required extensive amount of computational power for reconstruction. For instance, the first layer of the SRCNN algorithm requires 64 layer of image decomposition by means of pre-trained 2D filter kernels, while the under-sampling/up-sampling methods such as MaxFlat only decomposed the image using one-shot convolution using a separable 2D kernel coefficients. Up-sampled image using the Gaussian and Simoncelli filters provide ripple-free recovery. However, the texture details are smoothed and pixelated. Notice the hallucinated lines introduced by Savtizky-Golay due to the side-lobe artifacts on the stop-band. Such artifacts are directly related to the human perception error which indicates such filters are not suitable for this application. In contrast, MaxFlat approach recovers with much less halo artifacts and better detail preservation.

B. Canny Edge-Detection: Variant of First Order Derivative

In this section, we study the problem of the edge detection using Canny's algorithm [4] that has been widely applied in many computer vision applications. The method is constructed by three main phases to create an abstract level of image edge structures. First the smooth gradients of the image are obtained using Gaussian kernels along horizontal ($\theta = 0$) and vertical ($\theta = \pi/2$) directions. In the second stage, an edge thinning is applied by non-maximum suppression technique, and finally an edge tracking by hysteresis method is applied to find the connected strong gradients. For more detail on

the implementation of Canny's algorithms, please refer to the build-in MATLAB function `edge(I, 'canny')`.

Our contribution here is to replace the gradient calculation in the first stage of the algorithm by MaxFlat kernels defined in previous section. We choose two rotating directions $\theta = \{0, \pi/2\}$ to match the horizontal and vertical derivative kernels. The default value of the Gaussian scale is $\sigma = \sqrt{2}$ with tap-length filter size of $L = 8$ within the `edge` function. We used the same tap-length size and set the flatness degrees to $P_x = P_y = 2$ which corresponds to the cutoff frequency of the Gaussian. Furthermore, we deploy Simoncelli and Savitzky-Golay filters with similar tuning schemes to study their performances. Figure 4 demonstrates the results of Canny edge detection on *pirate* image applied by all four different gradient kernels. The figure also includes the gradient vector fields on the selected patch which contains a slanted edge structure. Ideally, the gradient vectors should be perpendicular to the edge direction. Notice the deviation of gradient fields using Simoncelli's filter. The Savitzky-Golay also creates a longer transition period from dark to the bright region in the image due to the side-lob artifacts of the filter. We have found MaxFlat filter creates much cleaner edges using the Canny's steps compared to Gaussian. Notice the vector fields perturbation on the white area of the image patch using Gaussian as opposed to MaxFlat. This complies with the discussion and analysis we made in Section III where Gaussian perturbs high frequencies, while MaxFlat contains minimal artifacts beyond the cutoff level i.e. stop-band.

C. Unsharp Masking: Variant of Second Order Derivative

In classical unsharp masking (UM) method, the image edges are enhanced by emphasizing high frequency information [1] using a highpass filter. UM is a variant of sharpening technique which is applied on a blurred image to accent the edges in one-shot convolution problem. This is obtained by calculating
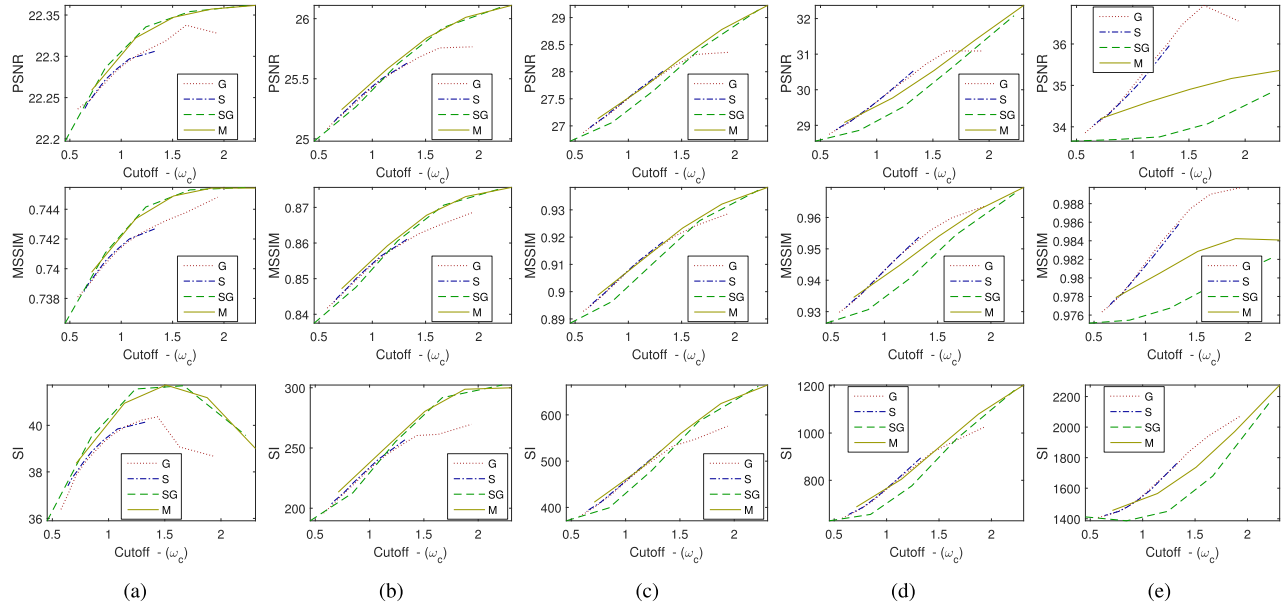
Fig. 5. Performance of unsharp masking on five blurred levels of LIVE image database (145 blurred images in total) using four different filters of Gaussian (G), Simoncelli (S), Savitzky-Golay (SG), and proposed MaxFlat (M). Their quality measure is averaged over 29 sharpened images in each blur level on different cutoff frequencies. The quality assessment is defined by two reference based measures of PSNR and MSSIM, and one no-reference based using SI. (a) Avg blur: $\bar{\sigma} = 4.74$. (b) Avg blur: $\bar{\sigma} = 1.8$. (c) Avg blur: $\bar{\sigma} = 1.25$. (d) Avg blur: $\bar{\sigma} = 0.94$. (e) Avg blur: $\bar{\sigma} = 0.60$.

the image Laplacian i.e. second partial derivatives which quadratically magnifies the frequency spectrum $|i\omega|^2$ along the horizontal and vertical axes. In general, UM is obtained by subtracting the scaled version of a highpass filtered image from the image itself i.e. $\bar{I} = I - \alpha\nabla^2 I$, where $\alpha \in [0, 1]$ is a positive scaling factor that tunes the strength of contrast enhancement. The common approach to employ the Laplacian operator is to utilize the second derivatives by Gaussian kernel with smoothness degree σ. As mentioned, this pitching factor mainly controls the range of perceived frequency and avoids noise or aliasing artifacts in reconstruction. Tweaking this scale low allows higher range of frequencies to be transferred, which is of importance in images that contain high frequency information.

Our main contribution here is to revise UM using the 2D MaxFlat kernels introduced in Section IV-A using different steering directions

$$\bar{I}(\Theta, P) = I - \alpha \sum_{\theta \in \Theta} I * K_{2D}(2, \theta, P_x, P_y) \qquad (15)$$

where Θ is the set of selected rotating directions for differentiation. In general, we can replace any lowpass derivative filters over MaxFlat to compare the utility of different methods.

The empirical analysis is done here on the LIVE image quality database [65], [68] which is distorted by Gaussian blur. The database consists of 29 color Kodak images and for every image five different blurring levels composed of 145 blurred images in total exist. The terms of evaluations are PSNR, MSSIM, and SI. These metrics, all together, identifies the integrity of UM solutions deployed by different kernels and lead us to a better quality judgment for reconstruction. We select steering kernels of Gaussian [12], [37], Simoncelli [32], and Savitzky-Golay [23]–[26] to compare

their utility as opposed to our proposed 2D MaxFlats. Figure 5 elaborates on sharpening 145 blurred images from LIVE database using all four 2D steering kernels. The quality measure is reported on different cutoff frequencies. At every cutoff level, we search for optimum index score obtained by different steering angle resolution $\Delta\theta = \{\frac{\pi}{2}, \frac{\pi}{4}, \frac{\pi}{6}, \frac{\pi}{8}\}$. The overall quantitative MaxFlat filter results compared to the state-of-the-art filter solutions reveal descent improvement over several quality measurements i.e. PSNR, MSSIM, and SI. Note that these values are the average results of 29 sharpened images (not single image result) implying that even small amount of improvement over the other methods is significant. As per the blur level decreases, higher cutoff frequencies are needed to achieve high quality performance. The rank observation here is mainly given to MaxFlat and Savitzky-Golay since they provide wider cutoff range solutions. MaxFlat offer even better quality reconstruction compared to Savtizky-Golay since it contains minimal stop-band artifacts. This is more evident on SI quality assessment which is non-reference based measure.

It is worth noting that the sharpening results achieved on less-blurred images (fifth category of blur level in LIVE) might sound controversial since both MaxFlat and Savitzky-Golay falls behind Gaussian and Simoncelli within the reference-based quality index measures i.e. MSSIM and PSNR. In fact sharpening such images with high cutoff frequencies over-sharpens them compared to their reference images. Although, the qualitative representation of the reconstructed images are high, the MSSIM and PSNR gains are poor. In contrary, the non-reference based SI measure yields higher performance on the MaxFlat and Savitzky-Golay using high cutoff filters. Table VI demonstrates such controversy by sharpening an example image from the fifth category of LIVE blurred image applied to low and high cutoff frequencies $\omega_c = \{1, 2.5\}$ (rad). As it can be observed, the MaxFlat

TABLE VI

UNSHARP MASKING ON BLUR LEVEL FIVE *Womenhat* FROM LIVE DATABASE USING FOUR DIFFERENT FILTERS OF GAUSSIAN, SIMONCELLI, SAVITZKY-GOLAY, AND PROPOSED MAXFLAT. TWO CUTOFF FREQUENCY RANGES ARE SET TO DESIGN FILTERS AND APPLIED ON THE BLURRED IMAGE. THE QUALITY INDEX IS REPORTED AS QI=[MSSIM,PSNR,SI] ON THE SHARPENED IMAGES
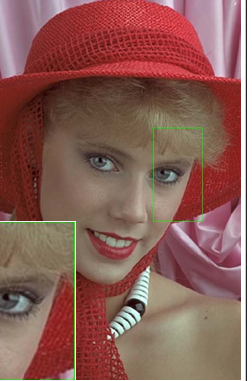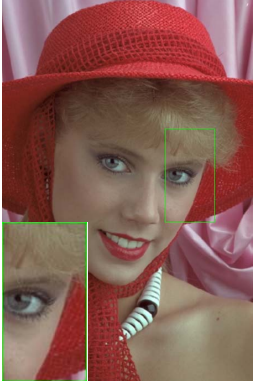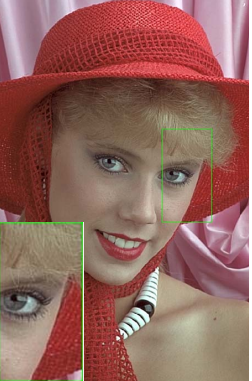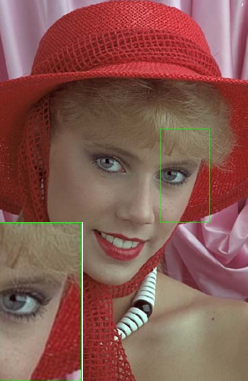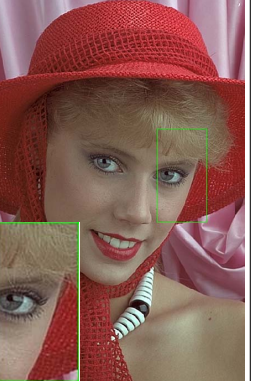
	Original ↓	Gaussian	Simoncelli	Savtizky-Golay	proposed MaxFlat
$\omega_c = 1$ (rad)		QI=[**0.9926**, **36.87**, **1353**]	QI=[0.9923, 36.69, **1304**]	QI=[0.9905, 35.68, 1092]	QI=[0.9920, 36.47, **1367**]
	Blurred ↓				
$\omega_c = 2.5$ (rad)	QI=[0.9906, 35.63, 1106]	QI=[0.9886, 27.28, 1988]	QI=[**0.9940**, **37.80**, 1576]	QI=[0.9915, 35.66, 2167]	QI=[0.9922, 35.96, **2425**]

TABLE VII

STATISTICAL SIGNIFICANCE TEST OF UNSHARP MASKING ON LIVE IMAGE DATABASE WITH 145 BLURRED IMAGES. THE SIGNIFICANCE OF QUALITY INDEX MEASURES OF PSNR, MSSIM, AND SI ARE MATCHED AGAINST PAIRWISE COLLECTION OF FOUR DIFFERENT APPROACHES OF GAUSSIAN (G), SIMONCELLI (S), SAVITZKY-GOLAY (SG), AND PROPOSED MAXFLAT (M). HERE THE FILTER METHODS IN COLUMNS ARE COMPARED AGAINST THE COMPETING APPROACHES IN ROWS

		G-Blurr level 1				G-Blurr level 2				G-Blurr level 3				G-Blurr level 4				G-Blurr level 5			
		G	S	SG	M	G	S	SG	M	G	S	SG	M	G	S	SG	M	G	S	SG	M
PSNR	Gaussian (G)	×	0	14	14	×	0	27	27	×	0	29	29	×	0	29	29	×	0	9	11
	Simoncelli (S)	29	×	29	29	29	×	29	29	29	×	29	29	29	×	29	29	29	×	14	16
	Savtizky-Golay (SG)	15	0	×	18	2	0	×	23	0	0	×	24	0	0	×	28	20	15	×	29
	MaxFlat (M)	15	0	11	×	2	0	6	×	0	0	5	×	0	0	1	×	18	13	0	×
	Total	59	0	54	61	33	0	62	79	29	0	63	82	29	0	59	86	67	28	23	56
MSSIM	Gaussian (G)	×	0	12	12	×	0	29	29	×	0	29	29	×	0	26	29	×	0	5	11
	Simoncelli (S)	29	×	29	29	29	×	29	29	29	×	29	29	29	×	29	29	29	×	13	20
	Savtizky-Golay (SG)	17	0	×	16	0	0	×	18	0	0	×	24	3	0	×	26	24	16	×	29
	MaxFlat (M)	17	0	13	×	0	0	11	×	0	0	5	×	0	0	3	×	18	9	0	×
	Total	63	0	54	57	29	0	69	76	29	0	63	82	32	0	58	84	71	25	18	60
SI	Gaussian (G)	×	1	19	21	×	0	29	29	×	0	29	29	×	0	29	29	×	0	20	23
	Simoncelli (S)	28	×	29	29	29	×	29	29	29	×	29	29	29	×	29	29	29	×	29	28
	Savtizky-Golay (SG)	10	0	×	12	0	0	×	10	0	0	×	19	0	0	×	25	9	0	×	28
	MaxFlat (M)	8	0	17	×	0	0	19	×	0	0	10	×	0	0	4	×	6	1	1	×
	Total	46	1	65	62	29	0	77	68	29	0	68	77	29	0	62	83	44	1	50	79

produced sharper edges on high cutoff frequency as opposed to the other approaches. Moreover, notice the brightness gained by Gaussian filter on $\omega_c = \{2.5\}$ in Table VI that is linked to the deviation of Gaussian filter response once the scale (variance) is decreased to obtain high cutoff frequency. This is one of the main drawbacks of the Gaussian that adds

(a) Original: SI = 747   (b) Gaussian (G)   (c) Simoncelli (S)   (d) Savitzky-Golay (SG)   (e) MaxFlat (M)

(f) G: SI = 1491   (g) S: SI = 1175   (h) SG: SI = 1348   (i) M: SI = 1418   (j) M (FB): SI = 1680

(k) RW [69]: SI = 1578   (l) EAW [69]: SI = 827   (m) MS [70]: SI = 704   (n) IC [71]: SI = 733   (o) MDF [72]: SI = 291

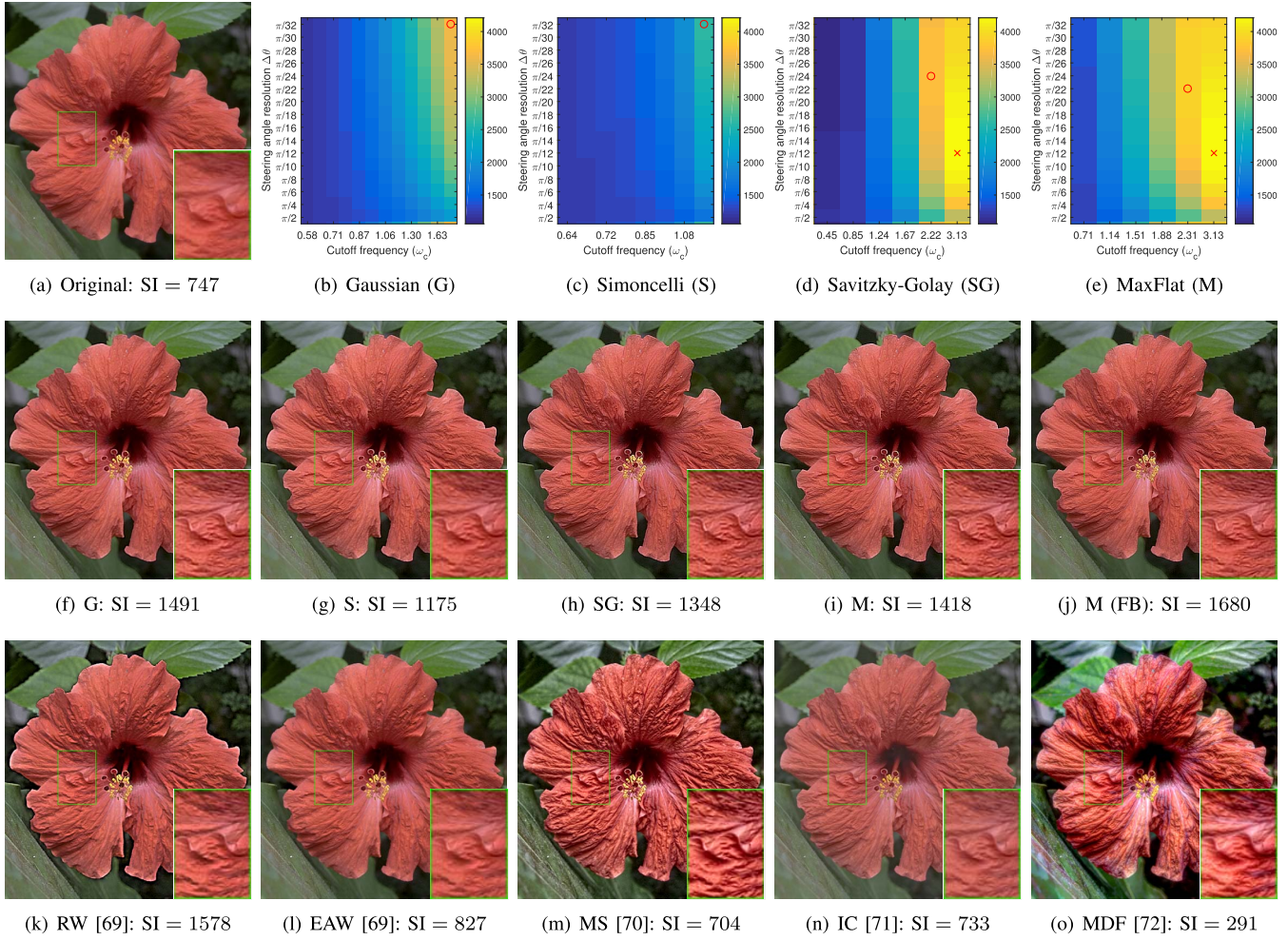Fig. 6. Unsharp masking performance on the *Flower* image using four different methods of Guassian, Simoncelli, Savitzky-Golay, and proposed MaxFlat filters. The shade of colors in (b)-(e) correspond to SI measure of sharpened images with various cutoff frequency parameters and different steering angle resolutions. The optimum performance of each method is found and are shown in (f)-(i). The optimum performance of the fullband (FB) (no-cutoff) sharpening using MaxFlat/Savitzky-Golay filter is also shown in (j). Images shown from (k) to (o) are related to non-linear edge-aware image enhancement methods.

constant (DC) components on the gray pixel values at such high cutoff levels. This can also be validated by observing the second derivative response of the Gaussian kernel in Table I. One way to fix this problem is to add another enhancing block after the sharpening by linear normalization of the image gray values. However, this is still not going to guarantee to balance the brightness level of the processed image compared to its original input image.

We conduct our last validation on LIVE image database by counting the statistical significant of all three quality indexes of PSNR, MSSIM, and SI by pair-wise matching of all four different filter methods. Table VII elaborates on this matching contest. For instance, within the fifth level category, which contains 29 blurred images, the Gaussian yields 18 significant sharpened images in terms of PSNR quality measure compared to MaxFlat. The number of significance for each method is found and compared to other competing approaches and accumulated in total. As can be seen, MaxFlat outranks the others in third and fourth blurred level by means of all quality index measures. In fifth category, MaxFlat outperforms in terms of SI measure, while falling behind the Gaussian in terms of PSNR and MSSIM. With respect to first and second categories, which

contain severe blurred images, MaxFlat is mainly significant in terms of reference based quality measures. However, it falls behind Savitzky-Golay approach evaluated on SI measure. This is simply because the high level blurred images contain limited low frequency information and Savitzky-Golay mainly perturbs non-informative high frequency structures in the image due to its side-lobe responses. So, as a consequence the SI turns to be sensitive to such false-positive information deduced by Savitzky-Golay filter.

Note that the blurring artifacts in LIVE database are artificially introduced and do not necessarily represent natural blur effect that is usually caused by either point spread function (PSF) characteristics of the optical lens in camera or introduced by focus miss-alignments during the acquisition setup. To further support the utility of the proposed MaxFlat filter kernels, we provide more experiments on image sharpening applied to natural blur effects. We select two images of *flower*[2] and *folded-shirt* from Garment dataset[3] [73]

---

[2] Available to download from http://www.cs.huji.ac.il/~raananf/projects/eaw/
[3] Available to download from http://clopema.felk.cvut.cz/color_and_depth_dataset.html

(a) Original: SI = 374   (b) Gaussian (G)   (c) Simoncelli (S)   (d) Savitzky-Golay (SG)   (e) MaxFlat (M)

(f) G: SI = 483   (g) S: SI = 550   (h) SG: SI = 479   (i) M: SI = 601   (j) M (FB): SI = 5
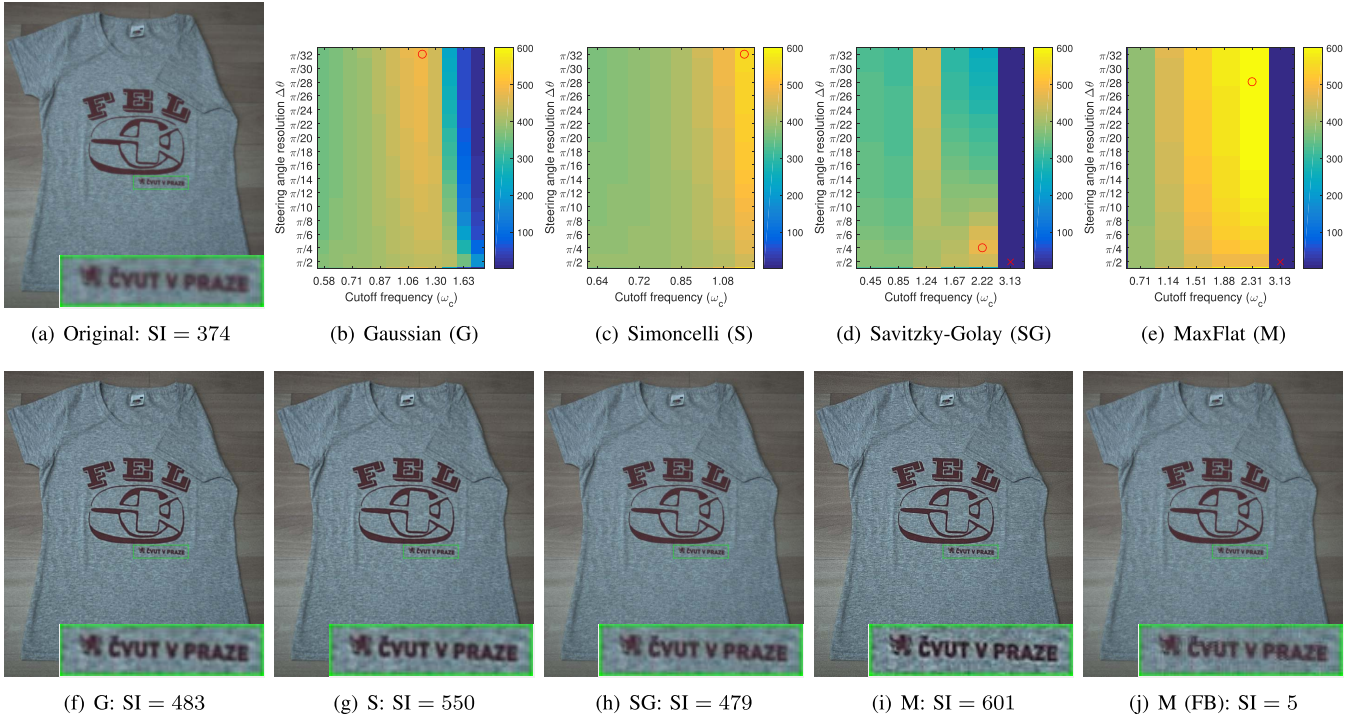
Fig. 7.   Unsharp masking performance on the *folded shirt* image using four different methods of Guassian, Simoncelli, Savitzky-Golay, and proposed MaxFlat filters. The shade of colors in (b)-(e) correspond to SI measure of sharpened images with various cutoff frequency parameters and different steering angle resolutions. The optimum performance of each method is found and are shown in (f)-(i). The optimum performance of the fullband (FB) (no-cutoff) sharpening using MaxFlat/Savitzky-Golay filter is also shown in (j).

(a) Original: SI = 4739   (b) Gaussian (G)   (c) Simoncelli (S)   (d) Savitzky-Golay (SG)   (e) MaxFlat (M)

(f) G: SI = 16347   (g) S: SI = 12037   (h) SG: SI = 14513   (i) M: SI = 15871   (j) M (FB): SI = 18862
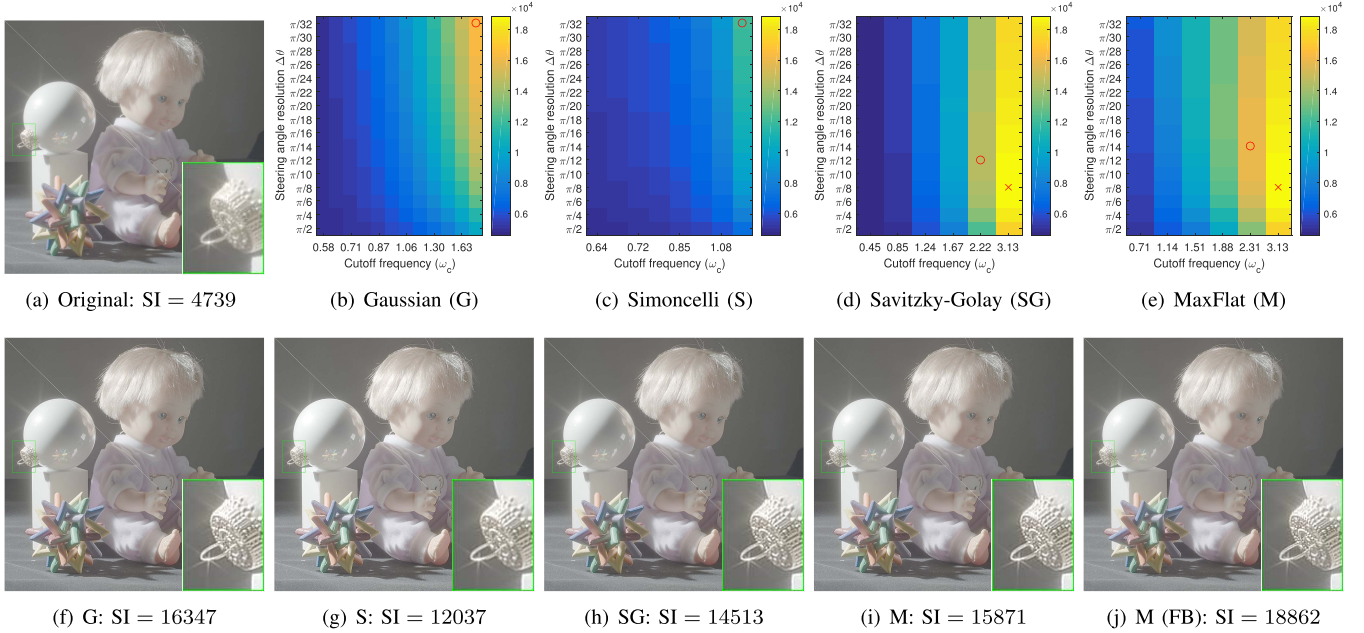
Fig. 8.   Unsharp masking performance on the *doll* HDR image using four different methods of Guassian, Simoncelli, Savitzky-Golay, and proposed MaxFlat filters. The shade of colors in (b)-(e) correspond to SI measure of sharpened images with various cutoff frequency parameters and different steering angle resolutions. The optimum performance of each method is found and are shown in (f)-(i). The optimum performance of the fullband (FB) (no-cutoff) sharpening using MaxFlat/Savitzky-Golay filter is also shown in (j).

restored in eight-bit levels, and one high-dynamic-range (HDR) image of *Doll*[4] [74]. All these three images are in raw non-compressed formats. It worth noting that these images have been extensively used as benchmark tests for variety of image enhancement methods in [69]–[72]. We conduct a heuristic analysis on all three images by varying different

steering angles and cutoff frequency of the deployed filters for unsharp masking. The SI quality index of the sharpened images are calculated for different parameter variations and demonstrated in Figures 6, 7, and 8 from (b) to (e). The optimum performance of all approaches are found i.e. maximum SI and the corresponding sharpened images are shown from (f) to (j) within the same figures. As can be observed, the MaxFlat filter applied for unsharp masking is outperforming

[4]Available to download from http://people.csail.mit.edu/yzli/

by preserving more detailed edges compared to the other filter methods. Regarding the *flower* image, we have also included the results from edge-aware enhancement methods in Figure 6 from (k) to (o) known as the interpolated convolution (IC) [71], regular-wavelet (RW) and edge-avoiding wavelets (EAW) [69], multi-scale (MS) tone and detail manipulation [70], and mixed-domain filtering (MDF) [72]. It worth noting that all these methods are non-linear approaches for detail enhancements and require high computation powers compared to linear convolution calculations applied in unsharp masking. Though the relative performance of these two different methodologies might not be a fair comparison, however it is interesting to see the level of detail manipulation of images compared in side-by-side. The non-linear approaches are mainly introduced to balance out between edge-preservation and detail smoothing within the images by regulating the relative information between spatial and pixel illumination. Whereas, in unsharp masking this is only done in the pixel illumination level. With regards to *doll* HDR image in 8 please note that we have used logarithmic scale on the image gray level for processing in order to balance out the tone-map of the image. We did not use any additional compression or histogram manipulation of the gray levels that usually taken place such as in [69]–[72]. This is simply to avoid the information loss in frequency details. The unsharp masking done by fullband differentiation (no cutoff) do not necessarily yields good quality reconstruction. While the sharpening quality of *flower* and *doll* outperform by fullband MaxFlat/Savtizky-Golay kernels, *folded shirt* in Figure 7 reveals poor quality recovery which the sharpened image is contaminated by noise/aliased information.

VI. CONCLUSION

We have developed a numerical framework based on maximally flat technique to design compact kernels of lowpass/fullband differentiators in a closed form solution that are sharply localized in the Fourier space. The kernels comprised of FIR filters in variety of derivative orders and cutoff frequencies. We extended our design by incorporating these filters into separable 2D kernels to obtain the directional differentiation of an image in arbitrary rotating angle. This compares favorably with the existing steerable filters in the literature [12], [32], [37] that are unable to set sharp cutoff ranges on higher frequencies. This is of paramount importance in applications where there is a need to transfer fine image structures with high-frequency information. In particular, we tested our 2D MaxFlat kernels in three different applications. The utility of zero order lowpass (interpolation) filter was studied in image interpolation problem. First order was also studied in Canny edge detection where superior results were achieved compared to competing filter solutions. Finally, the second order differentiation was studied in unsharp masking (UM) to sharpen images from their blurry observation. The overall results in all three applications suggested that the proposed kernels are robust towards different cutoff parameters. For instance, in UM, the existing methods rely on deploying a Gaussian kernel to approximate the Laplacian operator. The sensitivity of such kernels with respect to the scaling parameters makes them very challenging for accurate

reconstruction. This is, in fact, the main reason of introducing adaptive techniques in [1]–[3] to mitigate such deficiencies.

2D MaxFlat kernels could be of interest to broad audiences in image processing. The future work of this paper will study the applications in tensor field problems [15] to determine the structural orientation in medical images. They will emerge as a generic dictionary solutions in replacement over learning based approaches such as super-resolution methods in [3], [13], and [75]. They can be also investigated to derive features in computer vision problems such as SIFT and SURF [8]–[11], [76].

REFERENCES

[1] A. Polesel, G. Ramponi, and V. J. Mathews, "Image enhancement via adaptive unsharp masking," *IEEE Trans. Image Process.*, vol. 9, no. 3, pp. 505–510, Mar. 2000.

[2] G. Deng, "A generalized unsharp masking algorithm," *IEEE Trans. Image Process.*, vol. 20, no. 5, pp. 1249–1261, May 2011.

[3] Y. Romano, J. Isidoro, and P. Milanfar, "RAISR: Rapid and accurate image super resolution," *IEEE Trans. Comput. Imag.*, vol. 3, no. 1, pp. 110–125, Mar. 2017.

[4] J. Canny, "A computational approach to edge detection," *IEEE Trans. Pattern Anal. Mach. Intell.*, vol. PAMI-8, no. 6, pp. 679–698, Nov. 1986.

[5] P. Perona and J. Malik, "Scale-space and edge detection using anisotropic diffusion," *IEEE Trans. Pattern Anal. Mach. Intell.*, vol. 12, no. 7, pp. 629–639, Jul. 1990.

[6] F. Mokhtarian and A. Mackworth, "Scale-based description and recognition of planar curves and two-dimensional shapes," *IEEE Trans. Pattern Anal. Mach. Intell.*, vol. PAMI-8, no. 1, pp. 34–43, Jan. 1986.

[7] A. C. Jalba, M. H. F. Wilkinson, and J. B. T. M. Roerdink, "Shape representation and recognition through morphological curvature scale spaces," *IEEE Trans. Image Process.*, vol. 15, no. 2, pp. 331–341, Feb. 2006.

[8] T. Lindeberg, "Feature detection with automatic scale selection," *Int. J. Comput. Vis.*, vol. 30, no. 2, pp. 79–116, 1998.

[9] D. G. Lowe, "Distinctive image features from scale-invariant keypoints," *Int. J. Comput. Vis.*, vol. 60, no. 2, pp. 91–110, 2004.

[10] K. Mikolajczyk and C. Schmid, "A performance evaluation of local descriptors," *IEEE Trans. Pattern Anal. Mach. Intell.*, vol. 27, no. 10, pp. 1615–1630, Oct. 2005.

[11] H. Bay, A. Ess, T. Tuytelaars, and L. Van Gool, "Speeded-up robust features (SURF)," *Comput. Vis. Image Understand.*, vol. 110, no. 3, pp. 346–359, 2008.

[12] M. Jacob and M. Unser, "Design of steerable filters for feature detection using canny-like criteria," *IEEE Trans. Pattern Anal. Mach. Intell.*, vol. 26, no. 8, pp. 1007–1019, Aug. 2004.

[13] C. Dong, C. C. Loy, K. He, and X. Tang, "Image super-resolution using deep convolutional networks," *IEEE Trans. Pattern Anal. Mach. Intell.*, vol. 38, no. 2, pp. 295–307, Feb. 2016.

[14] M. Cimpoi, S. Maji, I. Kokkinos, and A. Vedaldi, "Deep filter banks for texture recognition, description, and segmentation," *Int. J. Comput. Vis.*, vol. 118, no. 1, pp. 65–94, May 2016.

[15] Z. Püspöki, M. Storath, D. Sage, and M. Unser, "Transforms and operators for directional bioimage analysis: A survey," in *Focus on Bio-Image Informatics*. Springer, 2016, pp. 69–93.

[16] P. Hill, A. Achim, M. E. Al-Mualla, and D. Bull, "Contrast sensitivity of the wavelet, dual tree complex wavelet, curvelet, and steerable pyramid transforms," *IEEE Trans. Image Process.*, vol. 25, no. 6, pp. 2739–2751, Jun. 2016.

[17] L. Cornelius, *Applied Analysis*. Englewood cliffs, NJ, USA: Prentice-Hall, 1956.

[18] C. Lanczos, *Applied Analysis*, New York, NY, USA: Dover, 1988.

[19] C. E. Duchon, "Lanczos filtering in one and two dimensions," *J. Appl. Meteorol.*, vol. 18, no. 8, pp. 1016–1022, 1979.

[20] C. Groetsch, "Lanczo's generalized derivative," *Amer. Math. Monthly*, vol. 105, no. 4, pp. 320–326, 1998.

[21] N. Burch, P. E. Fishback, and R. Gordon, "The least-squares property of the lanczos derivative," *Math. Mag.*, vol. 78, no. 5, pp. 368–378, Dec. 2005.

[22] T. J. McDevitt, "Discrete lanczos derivatives of noisy data," *Int. J. Comput. Math.*, vol. 89, no. 7, pp. 916–931, 2012.

[23] A. Savitzky and M. J. E. Golay, "Smoothing and differentiation of data by simplified least squares procedures," *Anal. Chem.*, vol. 36, no. 8, pp. 1627–1639, 1964.

[24] P. A. Gorry, "General least-squares smoothing and differentiation by the convolution (Savitzky–Golay) method," *Anal. Chem.*, vol. 62, no. 6, pp. 570–573, 1990.

[25] J. Luo, K. Ying, P. He, and J. Bai, "Properties of Savitzky–Golay digital differentiators," *Digit. Signal Process.*, vol. 15, no. 2, pp. 122–136, Mar. 2005.

[26] R. W. Schafer, "What is a Savitzky–Golay filter? [lecture notes]," *IEEE Signal Process. Mag.*, vol. 28, no. 4, pp. 111–117, Jul. 2011.

[27] J. Kaiser and R. Hamming, "Sharpening the response of a symmetric nonrecursive filter by multiple use of the same filter," *IEEE Trans. Acoust., Speech, Signal Process.*, vol. 25, no. 5, pp. 415–422, Oct. 1977.

[28] J. F. Kaiser and W. A. Reed, "Data smoothing using low-pass digital filters," *Rev. Sci. Instrum.*, vol. 48, no. 11, pp. 1447–1457, 1977.

[29] M. Mboup, C. Join, and M. Fliess, "Numerical differentiation with annihilators in noisy environment," *Numer. Algorithms*, vol. 50, no. 4, pp. 439–467, Apr. 2009.

[30] E. P. Simoncelli, "Design of multi-dimensional derivative filters," in *Proc. 1st Int. Conf. Image Process.*, vol. 1. Nov. 1994, pp. 790–794.

[31] H. Farid and S. P. Eero, "Computer analysis of images and patterns," *Optimally Rotation-Equivariant Directional Derivative Kernels*, S. Gerald, D. Kostas and P. Josef, Eds. Kiel, Germany: Springer, Sep. 1997, pp. 207–214.

[32] H. Farid and E. P. Simoncelli, "Differentiation of discrete multidimensional signals," *IEEE Trans. Image Process.*, vol. 13, no. 4, pp. 496–508, Apr. 2004.

[33] T. Möller, R. Machiraju, K. Mueller, R. Yagel, "Evaluation and design of filters using a Taylor series expansion," *IEEE Trans. Vis. Comput. Graphics*, vol. 3, no. 2, pp. 184–199, Apr. 1997.

[34] T. Möller, K. Mueller, Y. Kurzion, R. Machiraju, and R. Yagel, "Design of accurate and smooth filters for function and derivative reconstruction," in *Proc. IEEE Symp. Volume Vis.*, Oct. 1998, pp. 143–151.

[35] T. Möller, R. Machiraju, Y. Kurzion, K. Mueller, and R. Yagel, "Spatial domain filter design," Dept. Comput. Inf. Sci., Ph.D. dissertation, Ohio State Univ., Columbus, OH, USA, 1999.

[36] D. Marr and E. Hildreth, "Theory of edge detection," *Proc. Roy. Soc. London. B, Biol. Sci.*, vol. 207, pp. 187–217, Feb. 1980.

[37] W. T. Freeman and E. H. Adelson, "The design and use of steerable filters," *IEEE Trans. Pattern Anal. Mach. Intell.*, vol. 13, no. 9, pp. 891–906, Sep. 1991.

[38] R. Deriche, "Recursively implementing the Gaussian and its derivatives," Dept. Informat. Math., Ph.D. dissertation, INRIA, Rocquencourt, France, 1993.

[39] T. Lindeberg, "Generalized Gaussian scale-space axiomatics comprising linear scale-space, affine scale-space and spatio-temporal scale-space," *J. Math. Imag. Vis.*, vol. 40, no. 1, pp. 36–81, May 2011.

[40] T. Lindeberg, *Scale-Space Theory in Computer Vision*, vol. 256. Springer, 2013.

[41] T. Lindeberg. (2017). "Discrete approximations of affine Gaussian receptive fields." [Online]. Available: https://arxiv.org/abs/1701.02127

[42] I. W. Selesnick and C. S. Burrus, "Maximally flat low-pass FIR filters with reduced delay," *IEEE Trans. Circuits Syst. II, Analog Digit. Signal Process.*, vol. 45, no. 1, pp. 53–68, Jan. 1998.

[43] I. W. Selesnick and C. S. Burrus, "Generalized digital Butterworth filter design," *IEEE Trans. Signal Process.*, vol. 46, no. 6, pp. 1688–1694, Jun. 1998.

[44] I. W. Selesnick, "Low-pass filters realizable as all-pass sums: Design via a new flat delay filter," *IEEE Trans. Circuits Syst. II, Analog Digit. Signal Process.*, vol. 46, no. 1, pp. 40–50, Jan. 1999.

[45] I. W. Selesnick, "Maximally flat low-pass digital differentiator," *IEEE Trans. Circuits Syst. II, Analog Digit. Signal Process.*, vol. 49, no. 3, pp. 219–223, Mar. 2002.

[46] O. Herrmann, "On the approximation problem in nonrecursive digital filter design," *IEEE Trans. Circuit Theory*, vol. 18, no. 3, pp. 411–413, May 1971.

[47] I. Daubechies *et al.*, *Ten Lectures on Wavelets*, vol. 61. Philadelphia, PA, USA: SIAM, 1992.

[48] T. Cooklev and A. Nishihara, "Maximally flat fir filters," in *Proc. IEEE Int. Symp. Circuits Syst.*, May 1993, pp. 96–99.

[49] T. Cooklev, T. Yoshida, and A. Nishihara, "Maximally flat half-band diamond-shaped FIR filters using the Bernstein polynomial," *IEEE Trans. Circuits Syst. II, Analog Digit. Signal Process.*, vol. 40, no. 11, pp. 749–751, Nov. 1993.

[50] S. Samadi, A. Nishihara, and H. Iwakura, "Universal maximally flat lowpass FIR systems," *IEEE Trans. Signal Process.*, vol. 48, no. 7, pp. 1956–1964, Jul. 2000.

[51] S.-C. Pei and P.-H. Wang, "Closed-form design of maximally flat FIR Hilbert transformers, differentiators, and fractional delayers by power series expansion," *IEEE Trans. Circuits Syst. I, Fundam. Theory Appl.*, vol. 48, no. 4, pp. 389–398, Apr. 2001.

[52] A. L. da Cunha, J. Zhou, and M. N. Do, "The nonsubsampled contourlet transform: Theory, design, and applications," *IEEE Trans. Image Process.*, vol. 15, no. 10, pp. 3089–3101, Oct. 2006.

[53] R. T. Gregory, "A method for deriving numerical differentiation formulas," *Amer. Math. Monthly*, vol. 64, no. 2, pp. 79–82, Feb. 1957.

[54] B. Fornberg, "Generation of finite difference formulas on arbitrarily spaced grids," *Math. Comput.*, vol. 51, no. 184, pp. 699–706, 1988.

[55] I. R. Khan and R. Ohba, "Closed-form expressions for the finite difference approximations of first and higher derivatives based on Taylor series," *J. Comput. Appl. Math.*, vol. 107, no. 2, pp. 179–193, 1999.

[56] I. R. Khan and R. Ohba, "New design of full band differentiators based on Taylor series," *IEE Proc.-Vis., Image Signal Process.*, vol. 146, no. 4, pp. 185–189, Aug. 1999.

[57] I. R. Khan and R. Ohba, "New finite difference formulas for numerical differentiation," *J. Comput. Appl. Math.*, vol. 126, nos. 1–2, pp. 269–276, 2000.

[58] I. R. Khan, R. Ohba, and N. Hozumi, "Mathematical proof of closed form expressions for finite difference approximations based on Taylor series," *J. Comput. Appl. Math.*, vol. 150, no. 2, pp. 303–309, 2003.

[59] I. R. Khan and R. Ohba, "Taylor series based finite difference approximations of higher-degree derivatives," *J. Comput. Appl. Math.*, vol. 154, no. 1, pp. 115–124, 2003.

[60] J. Li, "General explicit difference formulas for numerical differentiation," *J. Comput. Appl. Math.*, vol. 183, no. 1, pp. 29–52, Nov. 2005.

[61] H. Z. Hassan, A. A. Mohamad, and G. E. Atteia, "An algorithm for the finite difference approximation of derivatives with arbitrary degree and order of accuracy," *J. Comput. Appl. Math.*, vol. 236, no. 10, pp. 2622–2631, Apr. 2012.

[62] L. R. Rabiner and R. W. Schafer, "On the behavior of minimax relative error fir digital differentiators," *Bell Syst. Tech. J.*, vol. 53, no. 2, pp. 333–361, Feb. 1974.

[63] A. Eisinberg and G. Fedele, "On the inversion of the Vandermonde matrix," *Appl. Math. Comput.*, vol. 174, no. 2, pp. 1384–1397, Mar. 2006.

[64] H. S. Hou and H. Andrews, "Cubic splines for image interpolation and digital filtering," *IEEE Trans. Acoust., Speech, Signal Process.*, vol. 26, no. 6, pp. 508–517, Dec. 1978.

[65] Z. Wang, A. C. Bovik, H. R. Sheikh, and E. P. Simoncelli, "Image quality assessment: From error visibility to structural similarity," *IEEE Trans. Image Process.*, vol. 13, no. 4, pp. 600–612, Apr. 2004.

[66] G. Blanchet and L. Moisan, "An explicit sharpness index related to global phase coherence," in *Proc. IEEE Int. Conf. Acoust., Speech Signal Process. (ICASSP)*, Mar. 2012, pp. 1065–1068.

[67] A. Leclaire and L. Moisan, "No-reference image quality assessment and blind deblurring with sharpness metrics exploiting Fourier phase information," *J. Math. Imag. Vis.*, vol. 52, no. 1, pp. 145–172, May 2015.

[68] H. R. Sheikh, M. F. Sabir, and A. C. Bovik, "A statistical evaluation of recent full reference image quality assessment algorithms," *IEEE Trans. Image Process.*, vol. 15, no. 11, pp. 3440–3451, Nov. 2006.

[69] R. Fattal, "Edge-avoiding wavelets and their applications," *ACM Trans. Graph.*, vol. 28, no. 3, Aug. 2009, Art. no. 22.

[70] Z. Farbman, R. Fattal, D. Lischinski, and R. Szeliski, "Edge-preserving decompositions for multi-scale tone and detail manipulation," *ACM Trans. Graph.*, vol. 27, no. 3, p. 67, 2008.

[71] E. S. L. Gastal and M. M. Oliveira, "Domain transform for edge-aware image and video processing," *ACM Trans. Graph.*, vol. 30, no. 4, p. 69, 2011.

[72] X. Y. Li, Y. Gu, S. M. Hu, and R. R. Martin, "Mixed-domain edge-aware image manipulation," *IEEE Trans. Image Process.*, vol. 22, no. 5, pp. 1915–1925, May 2013.

[73] W. Libor, D. Krejcova, and V. R. Smutny, "CTU color and depth image dataset of spread garments," Center Mach. Perception, Czech Tech. Univ., Tech. Rep. CTUCMP-2013-25, 2013.

[74] Y. Li, L. Sharan, and E. H. Adelson, "Compressing and companding high dynamic range images with subband architectures," *ACM Trans. Graph.*, vol. 24, no. 3, pp. 836–844, Jul. 2005.

[75] S. Schulter, C. Leistner, and H. Bischof, "Fast and accurate image upscaling with super-resolution forests," in *Proc. IEEE Conf. Comput. Vis. Pattern Recognit.*, Jun. 2015, pp. 3791–3799.

[76] E. Saad and K. Hirakawa, "Defocus blur-invariant scale-space feature extractions," *IEEE Trans. Image Process.*, vol. 25, no. 7, pp. 3141–3156, Jul. 2016.
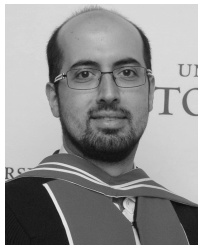
Mahdi S. Hosseini received the B.Sc. (*cum laude*) degree from the University of Tabriz in 2004, the M.Sc. degree from the University of Tehran in 2007, the M.A.Sc. degree from the University of Waterloo in 2010, and the Ph.D. degree from the University of Toronto (UofT) in 2015, all in electrical engineering. He is currently a Post-Doctoral Fellow with UofT and an Imaging Scientist with Huron Digital Pathology, Waterloo, ON, Canada. He also leads a Research Team of UofT students for Research and Development of the image analysis pipelines required in digital pathology scanning solutions. His research interest includes forward and inverse imaging problems, numerical differentiation, and kernel design for image analysis. He has served as a Reviewer of the IEEE Transaction on Image Processing, the IEEE Transaction on Signal Processing, and IEEE Transactions on Circuits and Systems for Video Technology.

Konstantinos N. Plataniotis (S'93–M'95–SM'03–F'12) has served as the Director of the Knowledge Media Design Institute, University of Toronto, from 2010 to 2012. He is currently a Professor and the Bell Canada Chair in multimedia with the ECE Department, University of Toronto. He is also the Founder and an Inaugural Director-Research of the Identity, Privacy and Security Institute, University of Toronto. His research interests are knowledge and digital media design, multimedia systems, biometrics, image and signal processing, communications systems, and pattern recognition. Among his publications in these fields are the recent books *WLAN Positioning Systems* (2012) and *Multi-Linear Subspace Learning: Reduction of Multidimensional Data* (2013). He is a registered Professional Engineer in Ontario and a fellow of the Engineering Institute of Canada. He was the Technical Co-Chair of the IEEE 2013 International Conference in Acoustics, Speech and Signal Processing. He was the IEEE Signal Processing Society Vice President for Membership from 2014 to 2016. He is the General Co-Chair of the 2017 IEEE GlobalSIP, the 2018 IEEE International Conference on Image Processing, and the 2021 IEEE International Conference on Acoustics, Speech and Signal Processing. He has served as the Editor-in-Chief of the IEEE Signal Processing Letters.